iScience

Article

tRF-Val-TAC-004 protects against renal ischemia-reperfusion injury via attenuating Apaf1-mediated apoptosis

Graphical abstract

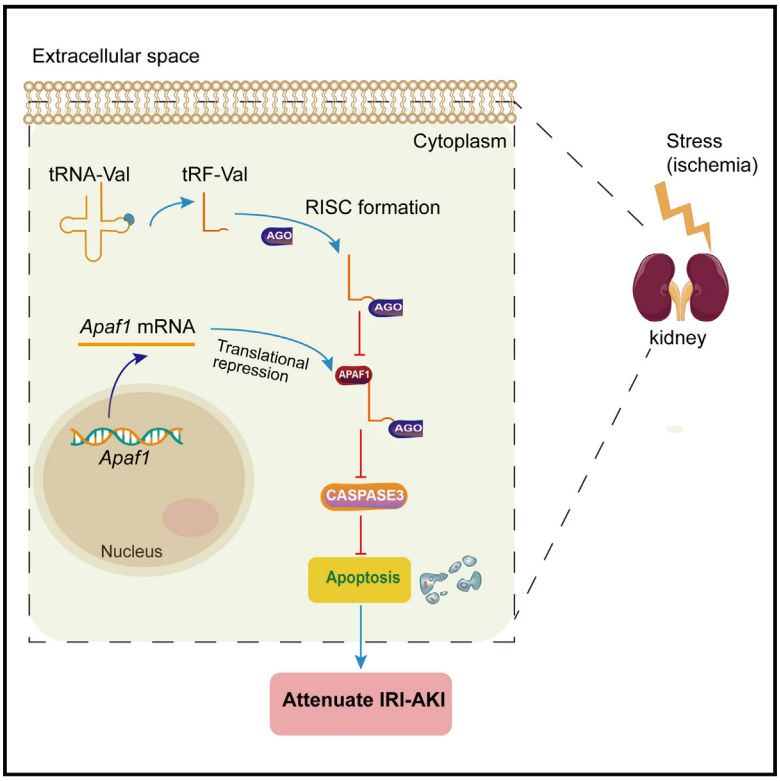

Highlights

- TRF-Val is downregulated in IRI-AKI mice and $CoCl_2$-treated BUMPT cells
- TRF-Val overexpression ameliorates the effects of apoptosis both *in vivo* and *in vitro*
- TRF-Val regulates Apaf1-mediated apoptosis through binding to AGO *in vitro*

Authors

Ni Yin, Xian Xie, Dan Li, ..., Yongzhong Tang, Hao Zhang, Wei Zhang

Correspondence

zhanghaoliaoqing@163.com (H.Z.), weizhangxy@126.com (W.Z.)

In brief

Molecular biology; Cell biology

Yin et al., 2025, iScience *28*, 111954
March 21, 2025
https://doi.org/10.1016/j.isci.2025.111954

CellPress

iScience

CellPress
OPEN ACCESS

Article

tRF-Val-TAC-004 protects against renal ischemia-reperfusion injury via attenuating Apaf1-mediated apoptosis

Ni Yin,[1,2] Xian Xie,[1,2] Dan Li,[1,2] Shikun Yang,[1,2] Yan Liu,[1,2] Yongzhong Tang,[3] Hao Zhang,[1,2,4,*] and Wei Zhang[1,2,4,5,*]
[1]Department of Nephrology, The Third Xiangya Hospital, Central South University, Changsha, Hunan 410013, China
[2]Clinical Research Center for Critical Kidney Disease in Hunan Province, Changsha, Hunan 410013, China
[3]Department of Anesthesiology, The Third Xiangya Hospital, Central South University, Changsha, Hunan 410013, China
[4]These authors contributed equally
[5]Lead contact
*Correspondence: zhanghaoliaoqing@163.com (H.Z.), weizhangxy@126.com (W.Z.)
https://doi.org/10.1016/j.isci.2025.111954

SUMMARY

tRNA-derived fragments (tRFs) play critical roles in cellular process, and we have previously reported that tRFs are involved in ischemia reperfusion injury induced acute kidney injury (IRI-AKI). However, the precise involvement of tRFs in IRI-AKI remains obscure. This study aims to elucidate the impact of tRF-Val-TAC-004 (tRF-Val) on IRI-AKI and uncover the underlying mechanisms. Our observations reveal a significant downregulation of tRF-Val in IRI-AKI mice and its overexpression mitigated renal dysfunction, morphological damage, and apoptosis in IRI-AKI mice, while its inhibition exacerbated these effects. Similar outcomes were replicated in $CoCl_2$-treated BUMPT cells upon transfection with tRF-Val mimic or inhibitor. Mechanistically, dual-luciferase reporter assay and AGO-RIP qPCR analyses demonstrated that tRF-Val suppresses Apaf1 expression by targeting the 3′-UTR of *Apaf1* mRNA. Furthermore, the protective efficacy of tRF-Val was notably weakened by *Apaf1*-overexpressing plasmids. In summary, these novel findings unveil the protective role of tRF-Val against IRI-AKI through inhibition of Apaf1-mediated apoptosis.

INTRODUCTION

Acute kidney injury (AKI) represents a prevalent critical condition affecting approximately 10–15% of hospitalized patients and exceeding 30% in intensive care units.[1] Ischemia-reperfusion injury stands out as a primary instigator of AKI, inciting oxidative stress, inflammatory responses, and cell death.[2] Within this context, the apoptosis of tubular epithelial cells (TECs) emerges as a crucial factor propelling AKI advancement, with anti-apoptotic strategies holding promise for impeding the transition from AKI to chronic kidney disease (CKD).[3,4] Central to the apoptotic cascade is apoptotic protease activating factor 1 (*Apaf1*), a pivotal component orchestrating apoptosis by activating procaspase-9 post cytochrome *c* release from mitochondria.[5] Nevertheless, the precise role of *Apaf1* in IRI-AKI remains enigmatic.

In recent years, tRNA-derived small non-coding RNAs (tsRNAs) have garnered substantial attention in disease investigations.[6] Within this category, tRNA halves (tiRNAs) and tRFs have been identified. Noteworthy functions of tRFs encompass transcriptional regulation[7] and translational repression.[8,9] Our prior investigations utilizing Illumina NextSeq 500 sequencing in kidney tissues exhibiting moderate to severe ischemic injury unveiled dysregulated tRFs, notably tRF-Val-TAC-004 (tRF-Val), within renal tissue of IRI-AKI mice.[10] This observation hinted at a potential involvement of tRFs in IRI-AKI; however, the specific role of tRF-Val in this context, particularly its impact on apoptosis, remains obscure.

Herein, through an *in vivo* IRI-AKI mouse model and an *in vitro* $CoCl_2$-treated TECs model, we identified a marked reduction of tRF-Val in renal IRI tissues, correlating with the severity of kidney injury in IRI-AKI. Mechanistically, our investigations unveil tRF-Val as a potential safeguard against TECs apoptosis in IRI-AKI, partially achieved through the inhibition of Apaf1 expression. These findings furnish novel insights into the molecular underpinnings and prospective therapeutic targets implicated in the onset and progression of IRI-AKI.

RESULTS

tRF-Val is significantly downregulated in renal tissue of IRI-AKI mice and $CoCl_2$-treated BUMPT cells

Previously, we have performed tRFs & tiRNAs sequencing assay on renal tissues and reported the involvement of tRFs and tiRNAs in IRI-AKI.[10] Herein, we subsequently analyzed the differential expressed tRFs with heatmap and volcano plot (Figures 1A and 1B). Among those dysregulated tRFs, we found that tRF-Val were aberrantly downregulated in IRI-AKI mice kidney (Figure 1C and Table 1). In addition, for a more intuitive understanding, we constructed the two-dimensional structure and

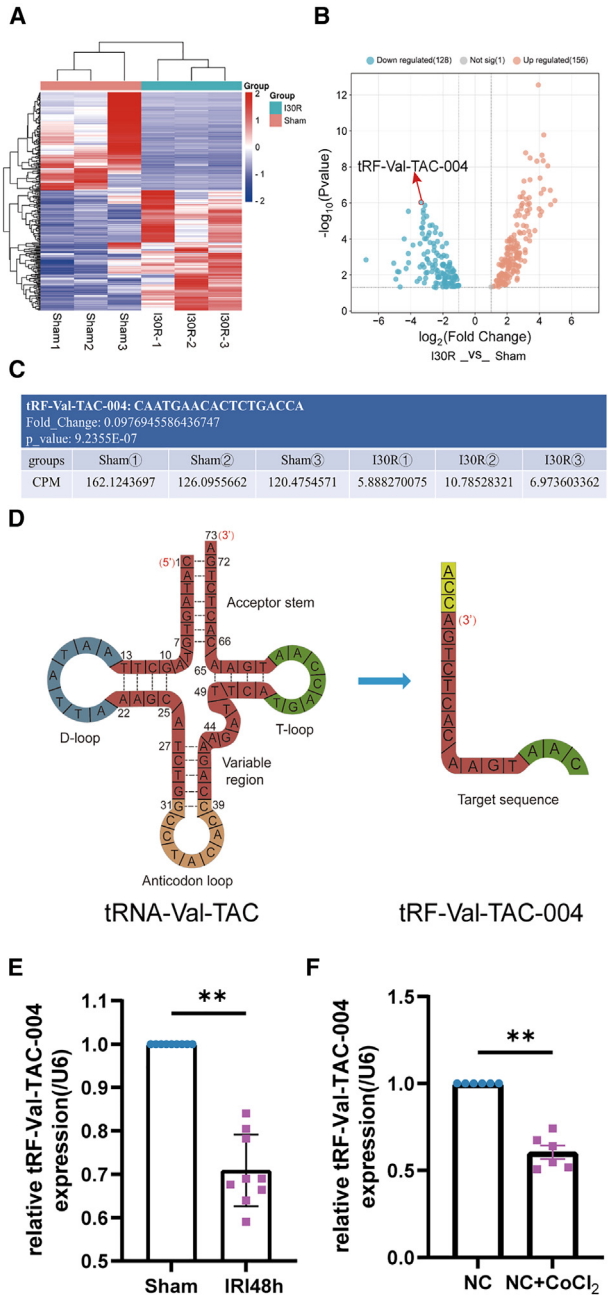

Figure 1. tRF-Val is significantly downregulated in renal IRI model both *in vivo* and *in vitro*

(A) Heatmap revealed the differential expression of tRFs in renal IRI tissues.
(B) Volcano map displayed the differential expression of tRFs in renal IRI tissues and tRF-Val was marked with red arrow.
(C) Expression of tRF-Val in tRFs sequencing.
(D) Structure and sequence diagram of tRNA-Val and tRF-Val.
(E) RT-qPCR verified the expression of tRF-Val in renal IRI tissue.
(F) RT-qPCR verified the expression of tRF-Val in $CoCl_2$-treated BUMPT cells. Data are represented as mean ± SEM.**, $p < 0.01$ versus respective vehicle. $n \geq 3$.

Table 1. The primer sequences used in this study

Primers	Sequence (5′ to 3′)
tRF-Val Forward	TGCTGCCGCAATGAACACT
tRF-Val Reverse	TATGGTTGTTCACGACTCCTTCAC
U6 Forward	GCTTCGGCAGCACATATACTAAAAT
U6 Reverse	CGCTTCACGAATTTGCGTGTCAT

sequence of tRF-Val and its parental tRNA-Val based on tRF database[11] (Figure 1D).Thereafter, we validated the expression of tRF-Val in IRI-AKI mouse models and $CoCl_2$-treated Boston university mouse proximal tubular (BUMPT) cells. Consistent with the previous tRF sequencing data, the RT-qPCR results showed that tRF-Val was robustly downregulated in IRI-AKI (ischemia for 30 min and reperfusion for 48 h) kidneys of C57BL/6J mice and $CoCl_2$-treated (48 h) BUMPT cells compared with the corresponding controls (Figures 1E and 1F). These data demonstrated that tRF-Val was downregulated in renal tubular cells in IRI-AKI model.

tRF-Val alleviates renal IRI and inhibits apoptosis

In order to clarify the effect of tRF-Val on renal TECs during IRI, we subsequently performed overexpressing assay by transfection of tRF-Val mimic in IRI-AKI mice, and the animal experiment design was depicted in the schematic diagram (Figure 2A). Compared with the negative control (NC) group, the mice treated with tRF-Val showed significantly lower serum creatinine (sCr) and blood urea nitrogen (BUN) levels after IRI challenge at both 24 h and 48 h (Figure 2B). Simultaneously, we also observed mitochondrial morphology in renal TECs at 24 h after reperfusion using transmission electron microscopy and the results demonstrated that the injection of tRF-Val mimic exerted nearly no effect on mitochondrial structure and integrity in the control group; however, disappearance of mitochondrial ridges and morphological disorder were observed in the IRI group, which was significantly ameliorated to certain extent after tRF-Val injection, suggesting a protective role of tRF-Val against mitochondrial damage (Figure 2C). Subsequently, we carried out RT-qPCR assay and the results indicated successful overexpression of tRF-Val (Figure 2D). Thereafter, we examined renal tissue damage via hematoxylin-eosin (HE) staining and periodic acid-Schiff (PAS) staining. Since the pathological injury and apoptosis were not prominent in the IRI24h model group (Figures S1A–S1D), then we further observed at 48 h after reperfusion. As shown in Figures 2E and 2F, kidneys from the Sham group showed normal renal structure. Notably, the tubular injuries including tubular necrosis and cast formation were observed after 48 h of reperfusion, which was mitigated in the tRF-Val-treated group. Furthermore, the TdT-mediated dUTP nick-end labeling (TUNEL) results showed an increase in green fluorescence compared to the Sham group in IRI48h model group, and a notable decrease after injecting tRF-Val (Figures 2G and 2H). In addition, our western blot results showed that pro-apoptotic protein cleaved caspase-3 was increased in IRI48h group, and its elevation was significantly repressed by tRF-Val. While the decreased expression of Bcl2 were significantly restored at least in part (Figures 2I and 2J).

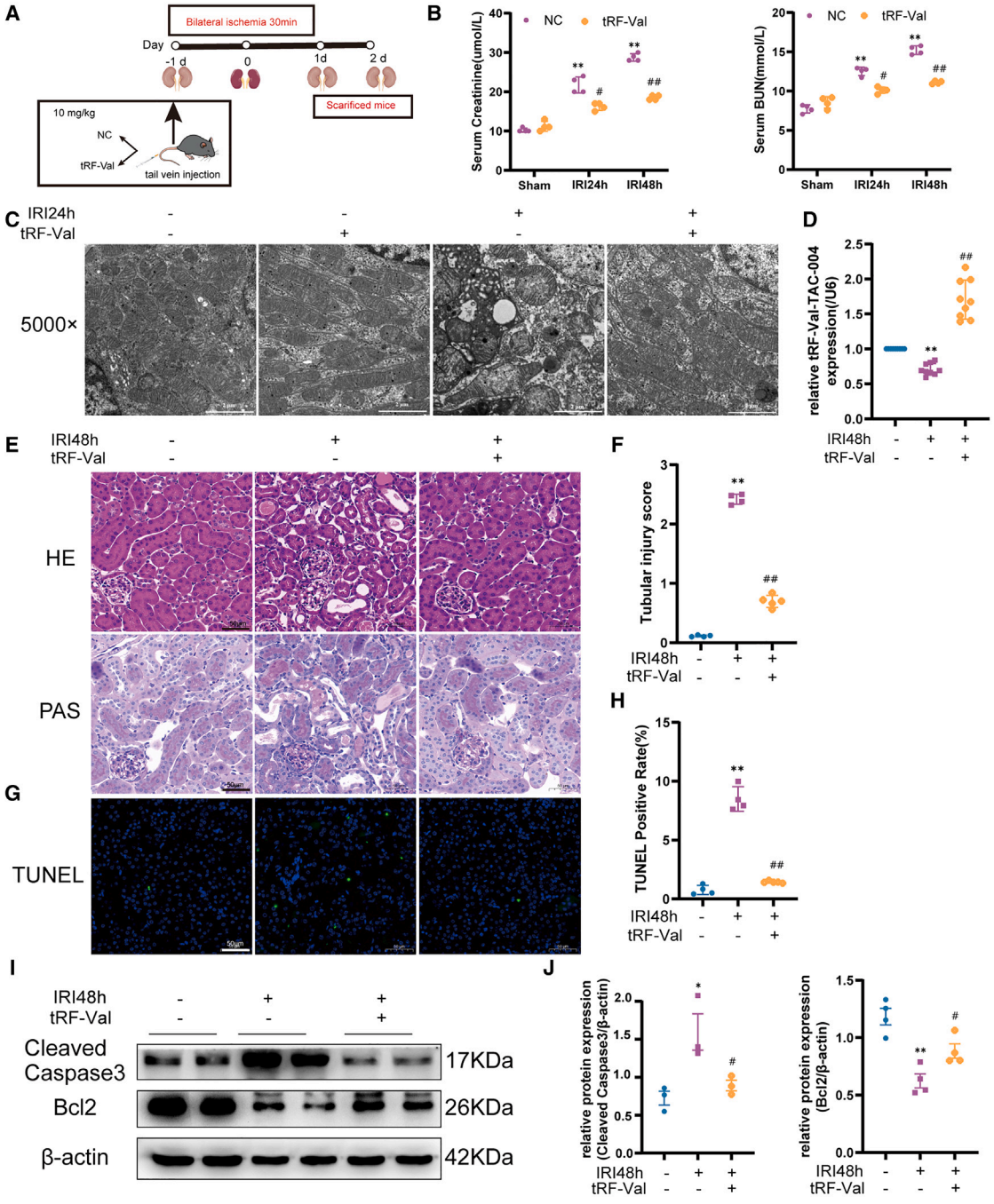

Figure 2. tRF-Val suppresses apoptosis during renal IRI

(A) Schematic diagram of the experimental procedure. NC or tRF-Val was injected via the caudal vein 24 h before bilateral ischemia for 30 min. Blood and kidney tissues were collected on day 1 or 2 after reperfusion for further analysis.

(B) sCr and BUN levels of indicated mice.

(C) Mitochondrial alteration was observed by transmission electron microscope (TEM) after IRI24h with or without tRF-Val injection. Scale Bar, 2 μm.

(D) tRF-Val expression by RT-qPCR in the renal cortex of mice after IRI48h with or without tRF-Val injection.

(E) Representative graphs of kidney sections with HE and PAS staining. Scale Bar, 50 μm.

(F) Quantitative analysis of tubular injury score.

(G) Representative images of kidney sections with TUNEL staining. Blue fluorescence indicates nuclear staining; Green fluorescence indicates cell death. Scale Bar, 50 μm.

(H) Quantification analysis of TUNEL-positive cells.

(I) Western blot analysis of Bcl2 and cleaved caspase-3 with β-actin as a loading control.

(J) Quantitative analysis of Bcl2 and cleaved caspase-3. Data are represented as mean ± SEM. *, $p < 0.05$ versus respective Sham-operated group; **, $p < 0.01$ versus respective Sham-operated group; #, $p < 0.05$ versus NC-treated IRI group; ##, $p < 0.01$ versus NC-treated IRI group. n = 3–5.

The previous results preliminarily showed that tRF-Val was protective against tubular injury in IRI-AKI. To further confirm the protection of tRF-Val, we continued to investigate whether the inhibitor of tRF-Val could aggravate tubular injury, as presented in Figure 3A. tRF-Val inhibitor further elevated sCr and BUN compared to IRI alone group, as shown in Figure 3B. The mitochondria were slightly swollen and vacuolated in the group of tRF inhibitor injection alone. In the IRI24h group, observations unveiled obvious swollen, vacuolated mitochondria reduced in number, disorganized in arrangement, and in some cases lacking mitochondrial ridges. Notably, in the IRI24h group treated with tRF-Val inhibitor injection, mitochondrial impairment was more severe, with a slightly widened perinuclear space, prevalent lysosomal granules within the mitochondrial matrix, as evidenced in Figure 3C. RT-qPCR data indicated successful inhibition of tRF-Val (Figure 3D). Following this, the HE and PAS staining revealed exacerbated tubular damage after tRF-Val inhibitor administration, characterized by the enhanced disappearance of brush border and formation of casts (Figures 3E and 3F). Concurrently, the TUNEL assay results exhibited a significant increase in green fluorescence after tRF-Val inhibitor administration (Figures 3G and 3H). Western blot analysis further revealed an elevation in the expression of cleaved caspase-3 in the IRI48h group, with a more pronounced increase post tRF-Val inhibitor injection, While the decreased expression of Bcl2 in IRI48h group were even lower with tRF-Val inhibitor treatment, aligning with the TUNEL outcomes (Figures 3I and 3J). This suggests that the inhibition of tRF-Val could exacerbate apoptosis of renal TECs during IRI-induced AKI. Collectively, these data demonstrate that tRF-Val plays a protective role in IRI-AKI.

tRF-Val attenuates cell apoptosis in BUMPT cells under $CoCl_2$ induction

The preceding results indicate that tRF-Val may exhibit anti-apoptotic properties in IRI-AKI mice *in vivo*. Consequently, we devised a hypoxia model using BUMPT cells to explore the impact of tRF-Val on hypoxic injury *in vitro*. As illustrated in the experimental schematic, we transfected tRF-Val or a NC into BUMPT cells 24 h prior to exposure to $CoCl_2$ (Figure 4A). RT-qPCR analysis confirmed successful transfection of tRF-Val into BUMPT cells (Figure 4B). Subsequent investigations involved a TUNEL assay to assess the influence of tRF-Val on BUMPT cell apoptosis *in vitro*, revealing an association between tRF-Val presence in BUMPT cells and a reduced rate of apoptosis (Figures 4C and 4D). To further validate the impact of tRF-Val on cell apoptosis, we employed flow cytometry techniques to observe the effect of transfecting tRF-Val on $CoCl_2$-induced cell apoptosis. Through labeling with PI and Annexin V- FITC, flow cytometry experiments revealed that tRF significantly reduced the level of apoptosis in renal TECs induced by $CoCl_2$ (Figures 4E and 4F).

Additionally, the western blot analysis indicated the occurrence of cell apoptosis under $CoCl_2$-induced hypoxia and illustrated that tRF-Val could partially ameliorate BUMPT cells apoptosis featured by decreased expression of cleaved caspase-3 and restored expression of Bcl2, aligning with the findings from the TUNEL staining and flow cytometry assay (Figures 4G and 4H).

e also introduced NC inhibitor and tRF-Val inhibitor 24 h prior to $CoCl_2$ treatment to observe the impact of the tRF-Val inhibitor on apoptosis in BUMPT cells (Figure 5A). Subsequently, we assessed the transfection efficacy of the tRF-Val inhibitor using RT-qPCR, validating the successful suppression of tRF-Val (Figure 5B). As expected, TUNEL staining revealed a slight increase in green fluorescence, though not statistically significant, in the group transfected solely with tRF-Val inhibitor. In contrast, a significant rise in green fluorescence was observed in the group treated with $CoCl_2$ following tRF-Val inhibitor transfection (Figures 5C and 5D). A similar result was obtained with the flow cytometry experiments (Figures 5E and 5F). Furthermore, western blot analyses further demonstrated a notable increase in the expression of cleaved caspase-3 and decreased Bcl2 in the group treated with $CoCl_2$ post tRF-Val inhibitor transfection compared to the group treated with $CoCl_2$ alone, aligning with the findings from the TUNEL assay (Figures 5G and 5H).

Collectively, these findings indicate that tRF-Val suppresses cells apoptosis in BUMPT cells under hypoxic stress conditions.

tRF-Val suppresses Apaf1 expression in IRI-AKI mice and $CoCl_2$-treated BUMPT cells

To clarify the downstream target genes of tRF-Val, we initiated mRNA sequencing by overexpression of tRF-Val in BUMPT cells (Figure 6A). Through bioinformatics analysis and KEGG enrichment assessment of the top 20 pathways, we identified the apoptotic pathway as a significant target influenced by tRF-Val. This discovery led to the generation of a heatmap displaying 13 differentially expressed genes associated with apoptosis (Figure 6B). Apaf1, recognized for its pivotal role in apoptosis and consistent expression patterns, was singled out as a potential target gene. Validation of Apaf1 expression via RT-qPCR revealed a consistent and downregulation after tRF-Val transfection, aligning with the sequencing data (Figure 6C and Table 2). Notably, both *in vivo* and *in vitro* models exhibited an upregulation of Apaf1 expression (Figures 6D and 6E).

We also conducted immunohistochemistry on renal tissues. The results validated a noticeable increase in Apaf1 expression in the kidneys of IRI48h mice, which was attenuated under tRF-Val administration (Figures 7A and 7B). Subsequently, western blot analysis of kidney tissue demonstrated a partial reduction observed upon tRF-Val intervention on IRI condition, consistent with the IHC results (Figures 7C and 7E). In BUMPT cells, tRF-Val and NC were transfected 24 h prior to $CoCl_2$ induction. Western blot results illustrated an increase in Apaf1 protein levels following treatment with $CoCl_2$ alone, which was markedly suppressed by tRF-Val (Figures 7D and 7F).

We also checked whether tRF-Val inhibitor functioned oppositely on the expression of Apaf1. As detected by immunohistochemistry, the expression of Apaf1 was increased upon IRI48h with tRF-Val inhibitor injection than IRI48h group alone (Figures 8A and 8B). Subsequently, western blot analysis showed that Apaf1 was indeed further increased following tRF-Val inhibitor injection compared with IRI48h group (Figures 8C and 8E). In addition, in BUMPT cell models transfected with tRF-Val inhibitor, and the result was consistent with the *in vivo* experiments (Figures 8D and 8F).

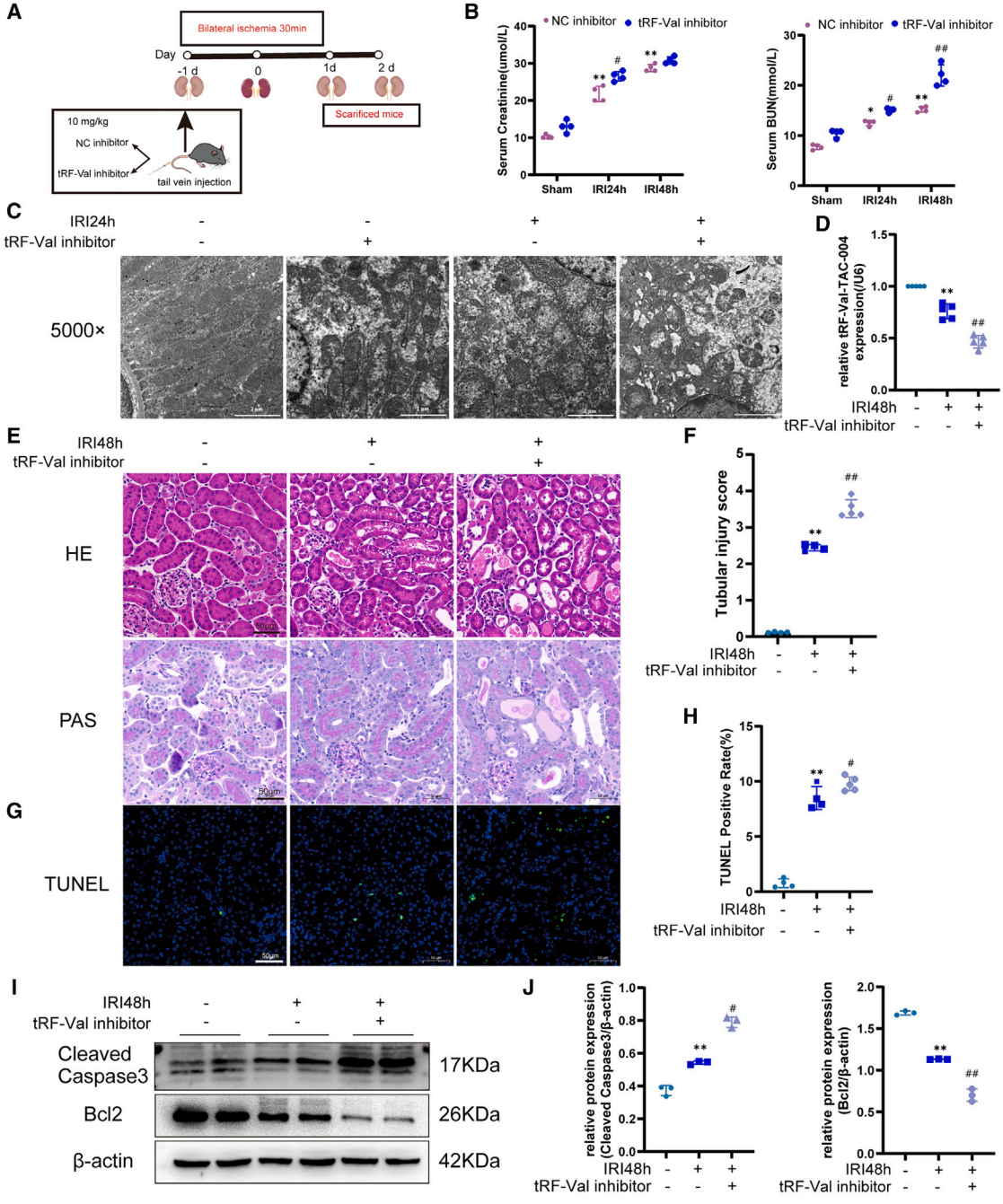

Figure 3. tRF-Val inhibitor exacerbates apoptosis during renal IRI

(A) Schematic diagram of the experimental procedure. NC inhibitor or tRF-Val inhibitor was injected via the caudal vein 24 h before bilateral ischemia for 30 min. Blood and kidney tissues were collected on day 1 or 2 after reperfusion for further analysis.

(B) sCr and BUN levels of indicated mice.

(C) Mitochondrial alteration was observed by TEM after IRI24h with or without tRF-Val inhibitor injection. Scale Bar, 2 μm.

(D) tRF-Val expression by RT-qPCR in the renal cortex of mice after IRI48h with or without tRF-Val inhibitor injection.

(E) Representative graphs of kidney sections with HE and PAS staining. Scale Bar, 50 μm.

(F) Quantitative analysis of tubular injury score.

(G) Representative images of kidney sections with TUNEL staining. Blue fluorescence indicates nuclear staining; Green fluorescence indicates cells death. Scale Bar, 50 μm.

(H) Quantification analysis of TUNEL-positive cells.

(I) Western blot analysis of Bcl2 and cleaved caspase-3 with β-actin as a loading control.

(J) Quantitative analysis of Bcl2 and cleaved caspase-3. Data are represented as mean ± SEM. *, $p < 0.05$ versus respective Sham-operated group; **, $p < 0.01$ versus respective Sham-operated group; #, $p < 0.05$ versus NC inhibitor-treated IRI group; ##, $p < 0.01$ versus NC inhibitor-treated IRI group. n = 3–5.

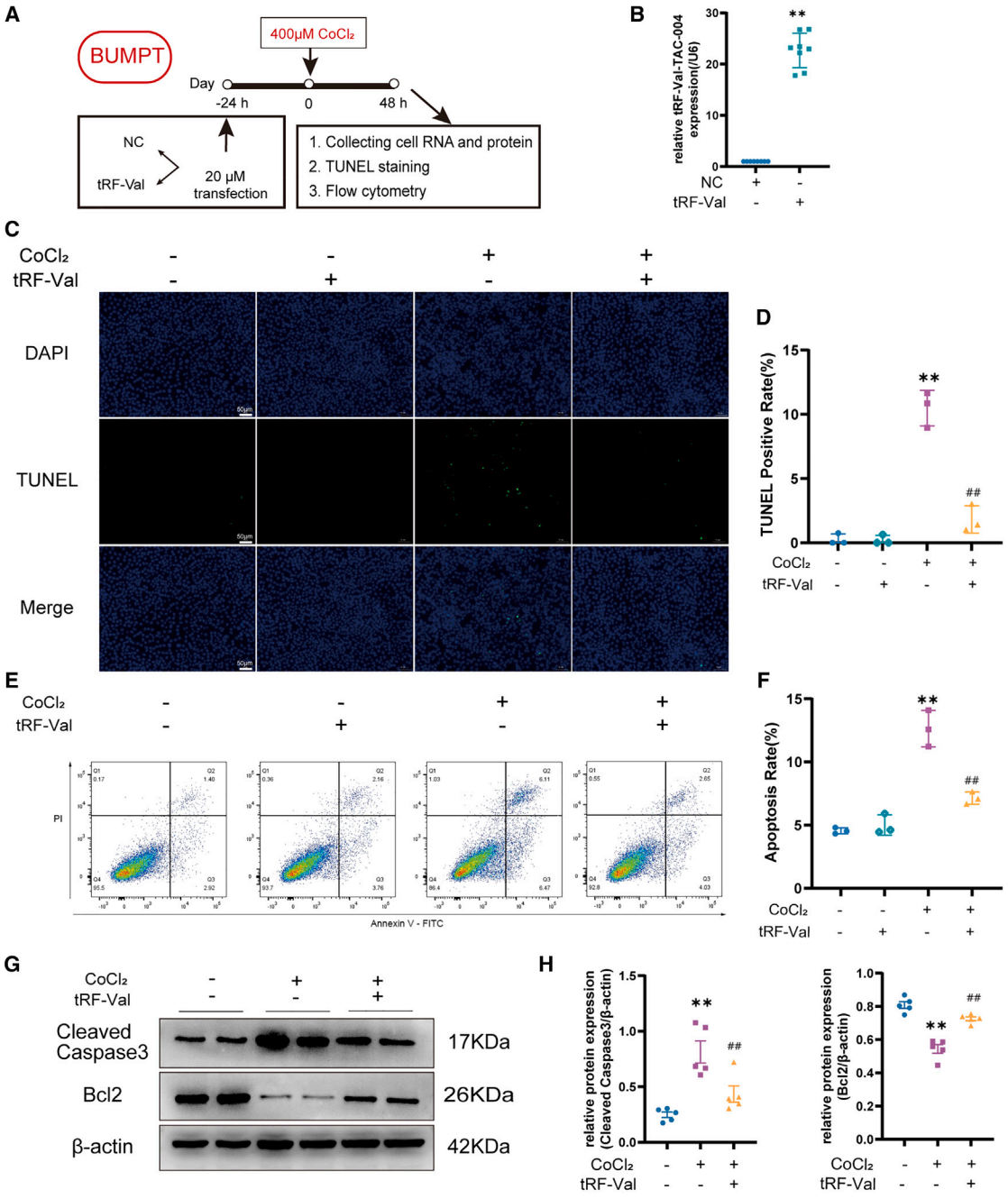

Figure 4. tRF-Val alleviates cellular death of BUMPT cells under $CoCl_2$ stress

(A) Schematic diagram of cells model. BUMPT cells were transfected with tRF-Val and NC, then were treated with $CoCl_2$ or vehicle for 48 h.

(B) Quantitative PCR analysis of tRF-Val expression.

(C) Representative images of TUNEL assay of BUMPT cells. Scale Bar = 50μm.

(D) Quantitative analysis of TUNEL-positive cells.

(E) Annexin V-FITC and PI flow cytometry analysis.

(F) Apoptosis rate analysis of flow cytometry.

(G) Western blot analysis of Bcl2 and cleaved caspase-3 with β-actin as a loading control.

(H) Quantitative analysis of Bcl2 and cleaved caspase-3. Data are represented as mean ± SEM. **, $p < 0.01$ versus respective vehicle; ##, $p < 0.01$ versus NC + $CoCl_2$ group. $n \geq 3$.

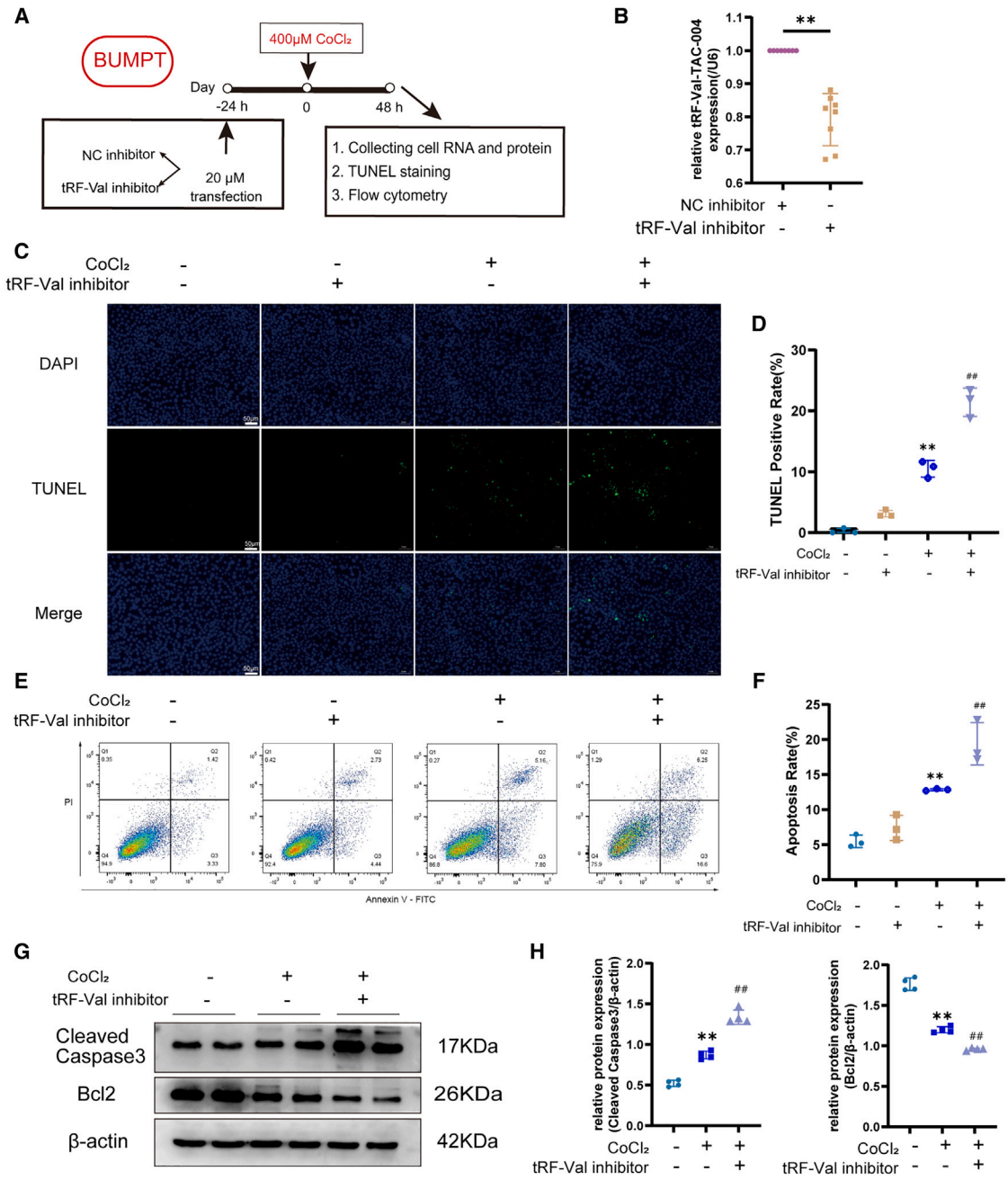

Figure 5. tRF-Val inhibitor aggravates cellular death of BUMPT cells under $CoCl_2$ stress

(A) Schematic diagram of cells model. BUMPT cells were transfected with tRF-Val inhibitor and NC inhibitor, then the cells were treated with $CoCl_2$ or vehicle for 48 h.

(B) Quantitative PCR analysis of tRF-Val expression.

(C) Representative images of TUNEL assay of BUMPT cells. Scale Bar, 50 μm.

(D) Quantitative analysis of TUNEL-positive cells.

(E) Annexin V - FITC and PI flow cytometry analysis.

(F) Apoptosis rate analysis of flow cytometry.

(G) Western blot analysis of Bcl2 and cleaved caspase-3 with β-actin as a loading control.

(H) Quantitative analysis of Bcl2 and cleaved caspase-3. Data are represented as mean ± SEM.**, $p < 0.01$ versus respective vehicle; ##, $p < 0.01$ versus NC inhibitor + $CoCl_2$ group. $n \geq 3$.

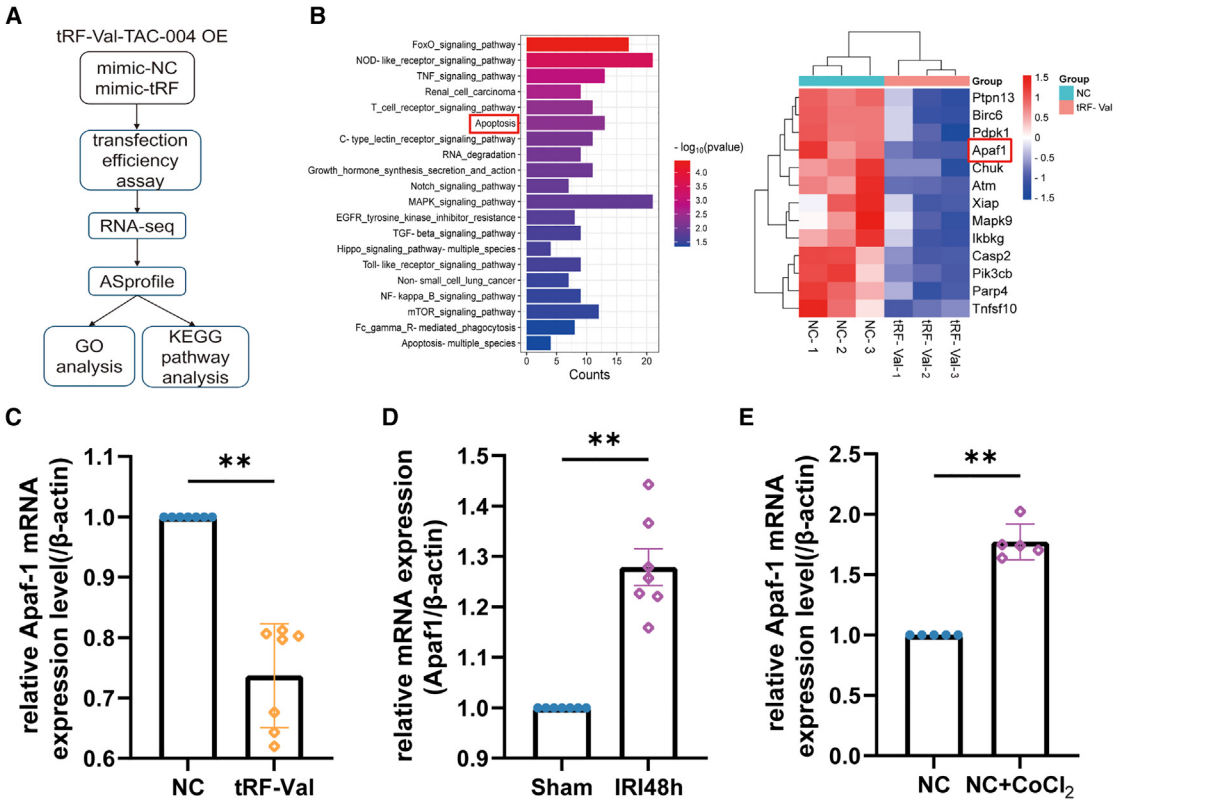

Figure 6. Apaf1 may be a target of tRF-Val in BUMPT cells

(A) Schematic diagram of mRNA sequencing.

(B) KEGG enrichment analysis of TOP 20 signaling pathways and heatmaps of 13 apoptosis-related genes. The key gene Apaf1 were marked with red rectangular box.

(C) RT-qPCR results of BUMPT cells transfection with NC or tRF-Val.

(D) RT-qPCR results of Apaf1 gene in tissue models.

(E) RT-qPCR results of Apaf1 gene in cell models. Data are represented as mean ± SEM.**$p < 0.01$ versus respective vehicle. $n \geq 3$.

Overall, the previous data indicated that Apaf1 might be a target of tRF-Val.

tRF-Val interacts with 3′-UTR of *Apaf1* mRNA

To elucidate the potential regulatory interactions between tRF-Val and *Apaf1*, we employed an online bioinformatic analysis tool to predict the binding site of tRF-Val within *Apaf1*. The analysis revealed a six-base complementary sequence within the 3′ untranslated region (UTR) of the *Apaf1* that paired with tRF-Val. Mutant sequences designed based on this finding were illustrated in Figure 9A. Subsequently, a dual luciferase reporter assay was conducted to validate the targeting of *Apaf1* mRNA by tRF-Val. Results indicated a significant decrease in luciferase activity in the WT-Apaf1 group following co-transfection with tRF-Val compared to the NC control, whereas the luciferase activity of the MUT-Apaf1 group remained largely unchanged (Figure 9B).

In addition, to investigate whether tRF-Val could bind with AGO protein, an Argonaute RNA immunoprecipitation (AGO-RIP) qPCR assay was conducted. Results demonstrated the binding of tRF-Val with AGO (Figure 9C). Collectively, our findings suggest that tRF-Val inhibited Apaf1 expression via targeting with the *Apaf1* mRNA 3′-UTR through binding with AGO.

Apaf1 overexpression weakens the effect of the tRF-Val on apoptosis in BUMPT cells

Here, we co-transfected tRF-Val and Apaf1 overexpression plasmids in BUMPT cells. The *Apaf1* plasmids design was shown in Figure 10A and it contained 9150 base pairs (bp). Meantime, we also tested the transfection efficacy of *Apaf1* plasmids, indicating that it was successfully transfected into BUMPT cells (Figure 10B). Subsequently, the TUNEL assay results showed that the green fluorescence increased in the group of *Apaf1* plasmids alone. As expected, the green fluorescence in co-transfection tRF-Val with *Apaf1* plasmids group was higher than that of $CoCl_2$-treated group after tRF-Val transfection (Figures 10C and 10D). Furthermore, we also detected *Apaf1* protein expression by western blot and results demonstrated that Apaf1 in both plasmids group and $CoCl_2$-treated group were substantially elevated compared with NC group. (Figures 10E and 10F). Thereby, we also observed that the cleaved caspase-3 were suppressed and Bcl2 were increased in $CoCl_2$-treated after tRF-Val transfection group compared with $CoCl_2$-treated alone group. However, this effect of tRF-Val in cleaved caspase-3 and Bcl2 were largely weakened after co-transfection *Apaf1* plasmids with tRF-Val (Figures 10G and 10H).

Table 2. The primer sequences used in this study

Primers	Sequence (5′ to 3′)
β-actin Forward	CAGAAGGAGATTACTGCTCTGGCT
β-actin Reverse	TACTCCTGCTTGCTGATCCACATC
Apaf1 Forward	AGTGGCAAGGACACAGATGG
Apaf1 Reverse	GGCTTCCGCAGCTAACACA

These data altogether confirm that tRF-Val represses cell apoptosis by inhibiting expression of Apaf1, at least partly.

DISCUSSION

This study unveils, for the first time, the downregulation of tRF-Val, a tRNA-derived small RNA fragment, in IRI-AKI mice and $CoCl_2$-induced BUMPT cells. Subsequent comprehensive investigations affirmed the protective role of tRF-Val against renal TECs apoptosis in the IRI-AKI model, both *in vivo* and *in vitro*.

A spectrum of experiments has initially illuminated the potential of tRFs as prognostic biomarkers for kidney diseases. Mishima et al. introduced novel insights into the constitutive alterations in tRNAs and their fragments, suggesting that tRFs could serve as early indicators of acute cellular injury.[12] Furthermore, previous research indicated that urinary exosomal tRFs could be novel diagnostic biomarkers for chronic kidney disease (CKD).[13] Notably, the elevation of tsRNAs in plasma preceded the rise of kidney injury molecule 1 (KIM-1) and creatinine in urine, hinting the potential of tsRNAs for early detection of renal injury.[14] Zhang Z et al. also highlighted the dysregulation of tRF-1:24-Glu-CTC-1 in podocyte injury induced by high glucose,

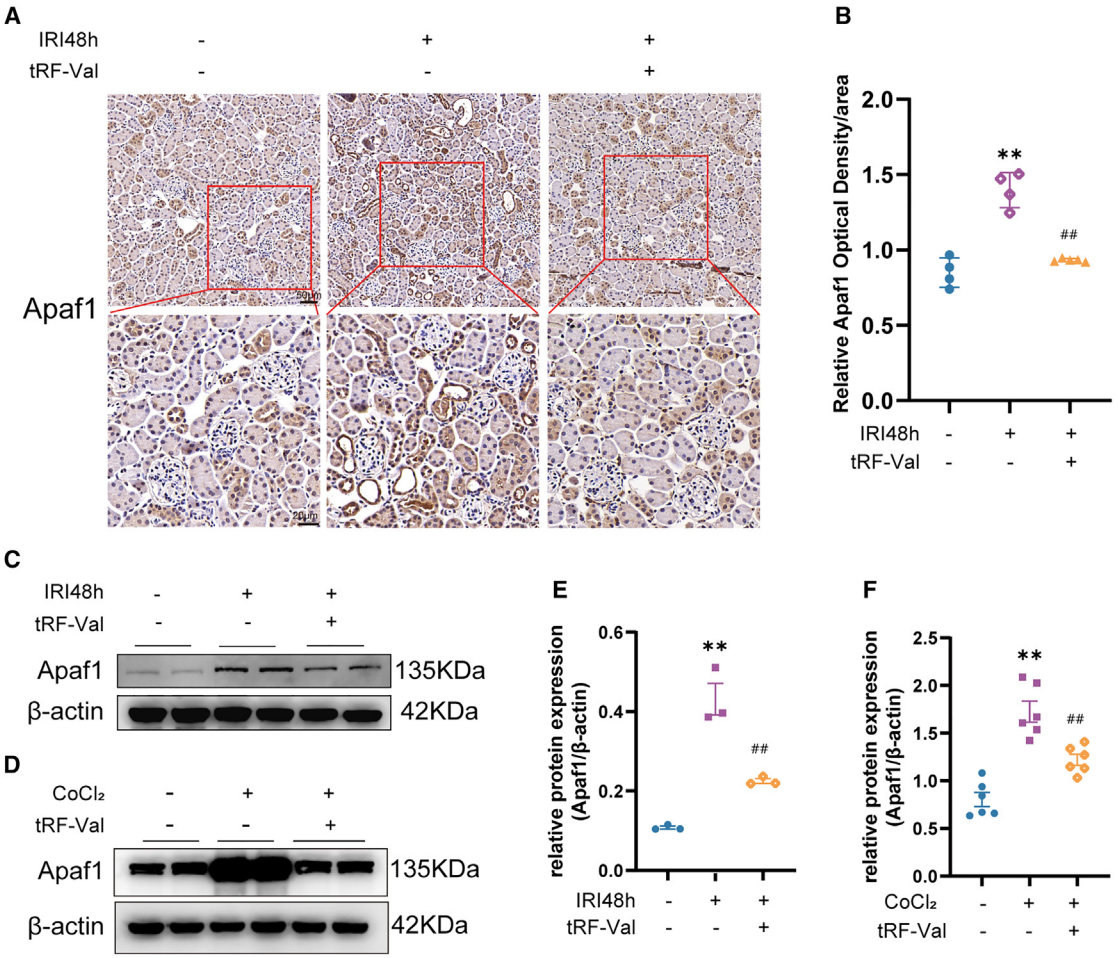

Figure 7. tRF-Val restrains Apaf1 expression in both renal IRI and $CoCl_2$-treated BUMPT cells

(A) Representative images of Apaf1 IHC results in IRI48h renal tissue with NC or tRF-Val injection. Scale Bar, 50 μm or 20 μm.

(B) Semi-quantitative analysis of Apaf1 IHC results.

(C) Western blot analysis of Apaf1 with β-actin as a loading control in IRI48h renal tissue with NC or tRF-Val injection.

(D) Western blot analysis of Apaf1 with β-actin as a loading control in BUMPT cells with NC or tRF-Val transfection.

(E) Quantitative analysis of Apaf1 in renal tissue.

(F) Quantitative analysis of Apaf1 in BUMPT cells. Data are represented as mean ± SEM. $^{**}p < 0.01$ versus respective vehicle; ##, $p < 0.01$ versus NC + $CoCl_2$ group or NC + IRI48h group. $n \geq 3$.

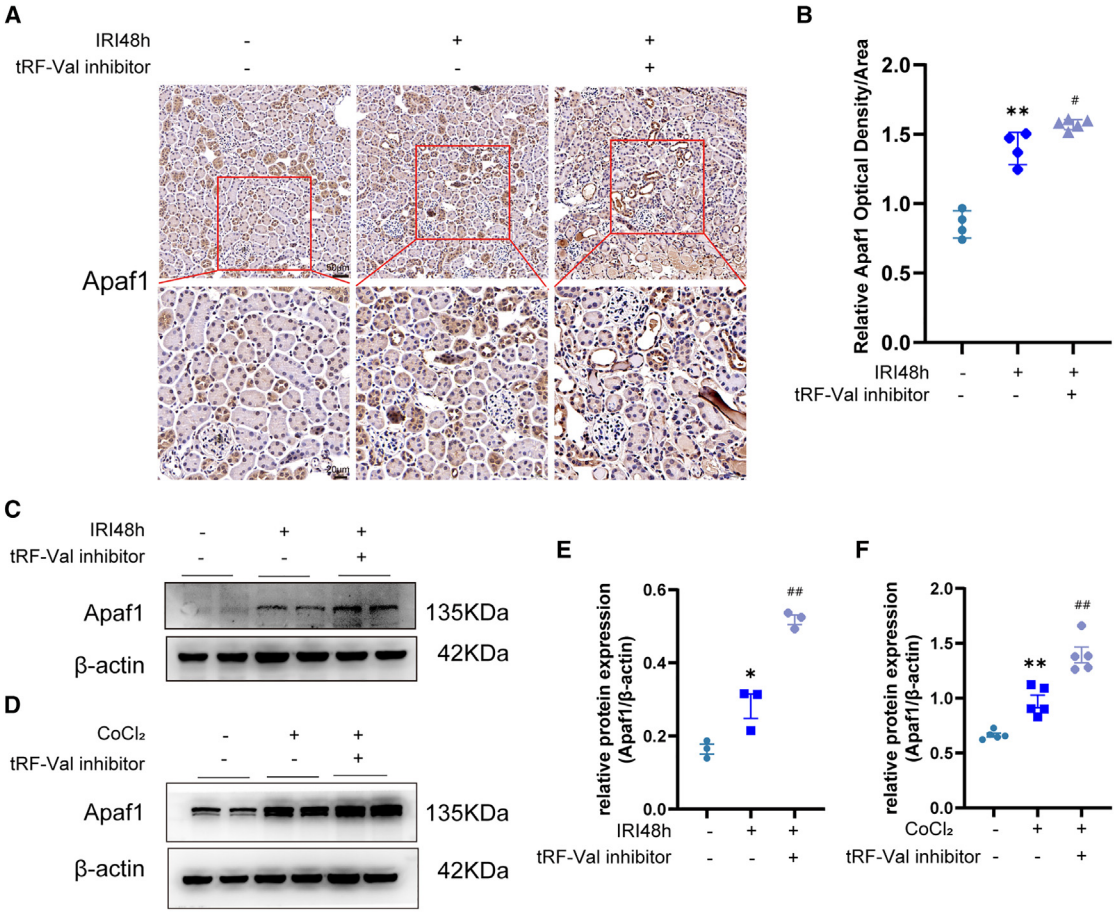

Figure 8. tRF-Val inhibitor preserves Apaf1 expression in both renal IRI and $CoCl_2$-treated BUMPT cells

(A) Representative images of Apaf1 IHC results in IRI48h renal tissue with NC inhibitor or tRF-Val inhibitor injection. Scale Bar, 50 μm or 20 μm.

(B) Semi-quantitative analysis of Apaf1 IHC results.

(C) Western blot analysis of Apaf1 with β-actin as a loading control in IRI48h renal tissue with NC inhibitor or tRF-Val inhibitor injection.

(D) Western blot analysis of Apaf1 with β-actin as a loading control in BUMPT cells with NC inhibitor or tRF-Val inhibitor transfection.

(E) Quantitative analysis of Apaf1 in renal tissue.

(F) Quantitative analysis of Apaf1 in BUMPT cells. Data are represented as mean ± SEM. *$p < 0.05$ versus respective vehicle; **$p < 0.01$ versus respective vehicle; #, $p < 0.05$ versus NC inhibitor + IRI48h group; ##, $p < 0.01$ versus NC inhibitor + $CoCl_2$ group or NC inhibitor + IRI48h group. $n \geq 3$.

proposing a potential biomarker for podocyte injury in diabetic kidney disease (DKD).[15]

This study pioneers the revelation that tRF-Val, a tRF-3, is significantly downregulated in both IRI-AKI and $CoCl_2$-treated BUMPT cells. This reduction correlates with renal functional decline and histological injury, suggesting that decreased expression may signify a hallmark of renal injury. However, the consistent downregulation of tRF-Val in other models of AKI (such as nephrotoxic drugs and sepsis-induced AKI) warrants further investigation.

In another way, we have recently reported that ischemia injury can induce tiRNA-Lys production which was mediated by *HIF-1* activation,[16] thus promoting the transcription of angiogenin, one of the key endoribonucleases during tRFs generation. However, despite the downregulation of tRF-Val in IRI-AKI, the precise factor leading to this reduction remains unclear. It is plausible that the decrease in tRF-Val could stem from the inhibition of tRNA-Val transcription or the downregulation of a specific endonuclease distinct from angiogenin. The internal mechanisms driving this process were not explored in this study.

Previous studies have elucidated that tRFs can exert their biological functions by impeding cell death. For instance, a study in gastric cancer by Cui H et al. revealed that a novel tRF-60:76-Val-CAC-2 promoted proliferation and suppressed apoptosis by targeting EEF1A1.[17] Furthermore, our research group recently demonstrated that tiRNA-Lys could cf. renoprotection in cisplatin-induced AKI by inhibiting ferroptosis through its interaction with the *GRSF1* protein.[16] Despite these insights, limited research has investigated the mechanisms through which tRFs offer protection against AKI. In our current study, we observed that tRF-Val could suppress apoptosis in renal TECs and mitigate IRI-AKI in both *in vivo* and *in vitro* models.

Apaf1, a central component of the mitochondrial apoptotic pathway, predominantly participates in the intrinsic pathway

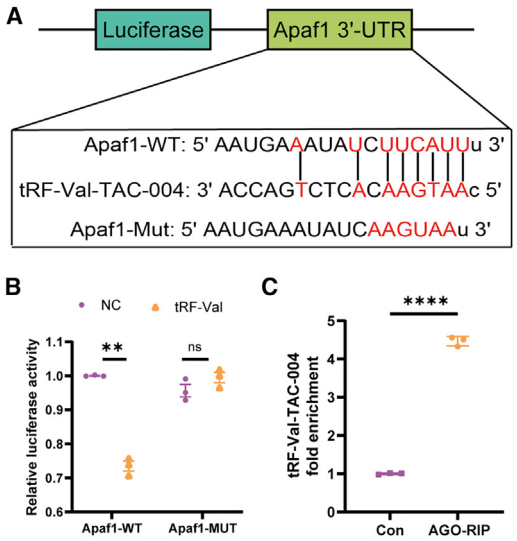

Figure 9. tRF-Val could bind 3′-UTR of *Apaf1* mRNA by loading with AGO

(A) The binding site between tRF-Val and Apaf1 predicted by the bioinformatics website and Apaf1-WT and Apaf1-MUT 3′-UTR were designed accordingly.

(B) The targeting relationship between tRF-Val and Apaf1 authenticated by dual-luciferase reporter gene assay.

(C) The binding relationship between AGO and tRF-Val verified by AGO-RIP qPCR. Data are represented as mean ± SEM. **, $p < 0.01$ versus Apaf1-WT + NC control; ****$p < 0.0001$ versus control. $n = 3$.

of apoptosis.[18] Its role involves binding with cytochrome *c* released from mitochondria, leading to caspase 9 activation, which subsequently triggers the activation of the key apoptotic enzyme, caspase-3.[5] Yang, H et al. have also demonstrated that the expression of Apaf1 is significantly upregulated in the rat ovaries IRI model and unilateral ureteral obstruction model.[19] Previous studies have demonstrated through *in vivo* and *in vitro* experiments that Apaf1 inhibitors hold promise for protecting against AKI.[20] In our investigation, we noted a significant upregulation of Apaf1 in IRI, which subsequently decreased following the administration or transfection of tRF-Val. These findings suggest that Apaf1 is likely the target of tRF-Val for inhibiting apoptosis.

Studies have reported that tRF-3s, ranging from 18 to 22 nucleotides in length, are independently generated by the Dicer enzyme and have the capability to enter the Argonaute-GW182-containing RNA-induced silencing complex (RISC), where they post-transcriptionally regulate mRNAs through sequence complementarity.[21] Kumar, P et al. conducted a meta-analysis of tRFs in human HEK-293T cells, revealing that tRFs share striking similarities with miRNAs, suggesting a significant role for tRFs in RNA silencing.[22] Notably, the tRF3008A, derived from tRNA-Val, has been documented to inhibit the metastasis and progression of colorectal cancer by disrupting the Wnt/β-catenin pathway in an AGO-dependent manner.[23] Meantime, tRF-03357 was significantly upregulated in high-grade serous ovarian cancer and could target the 3′-UTR of *HMBOX1* mRNA then promoting cell proliferation, migration and invasion.[24] Building upon these findings, we conducted a dual luciferase gene reporter assay and AGO-RIP qPCR experiment to validate the interaction between tRF-Val and Apaf1, confirming that tRF-Val effectively targets the 3′-UTR of *Apaf1* mRNA through sequence complementarity, aligning with previous reports.

In conclusion, our current study has elucidated the pivotal role of tRF-Val and its mechanism in IRI-AKI for the first time. Supporting our findings, we observed a decrease in tRF-Val levels during IRI-AKI, and overexpression of tRF-Val could mitigate IRI-AKI by suppressing apoptosis. This protective effect was mediated through the inhibition of Apaf1 by targeting 3′-UTR of its mRNA via sequence complementarity in an AGO-dependent manner. Our research offers new insights into the molecular mechanisms of tRFs in IRI-AKI, suggesting that tRF-Val could serve as a potential therapeutic target against IRI-AKI.

Limitations of the study

While our study has made significant strides, several potential limitations warrant acknowledgment. Firstly, beyond Apaf1 and apoptosis, our mRNA profiling indicated dysregulation of multiple target genes and pathways following tRF-Val overexpression, necessitating further exploration of other potential targets of tRF-Val and the interplay between tRF-Val and other forms of regulated cell death in future investigations. Secondly, the regulatory mechanism underlying the downregulation of tRF-Val remains unresolved. Lastly, we aim to incorporate clinical samples in our future research endeavors if feasible.

RESOURCE AVAILABILITY

Lead contact

Requests for further information and resources should be directed to and will be fulfilled by the lead contact, Wei Zhang (weizhangxy@126.com).

Materials availability

This study did not generate new unique reagents. Antibodies, reagents, and cell lines used were obtained from commercial or other sources as outlined in the key resources table.

Data and code availability

- mRNA-seq data have been deposited at GEO and are publicly available as of the date of publication. Original western blot images and microscopy data reported in this paper will be shared by the lead contact upon request.
- This paper does not report original code.
- Any additional information required to reanalyze the data reported in this paper is available from the lead contact upon request.

ACKNOWLEDGMENTS

This research was supported by grants from the National Natural Science Foundation of Hunan Province [No.2021JJ40954]. The corresponding author had full access to all the data in this study and was ultimately responsible for the decision to submit them for publication.

AUTHOR CONTRIBUTIONS

Conceptualization, W.Z., H.Z. and N.Y.; methodology, W.Z., N.Y., X.X., and D.L.; investigation, N.Y. and X.X.; writing-original draft, N.Y.; writing—review and editing, H.Z., W.Z., N.Y., X.X., D.L., S.Y., Y.L., and Y.T.; funding acquisition, W.Z. and H.Z.; resources, W.Z. and H.Z.; supervision, W.Z. and H.Z.

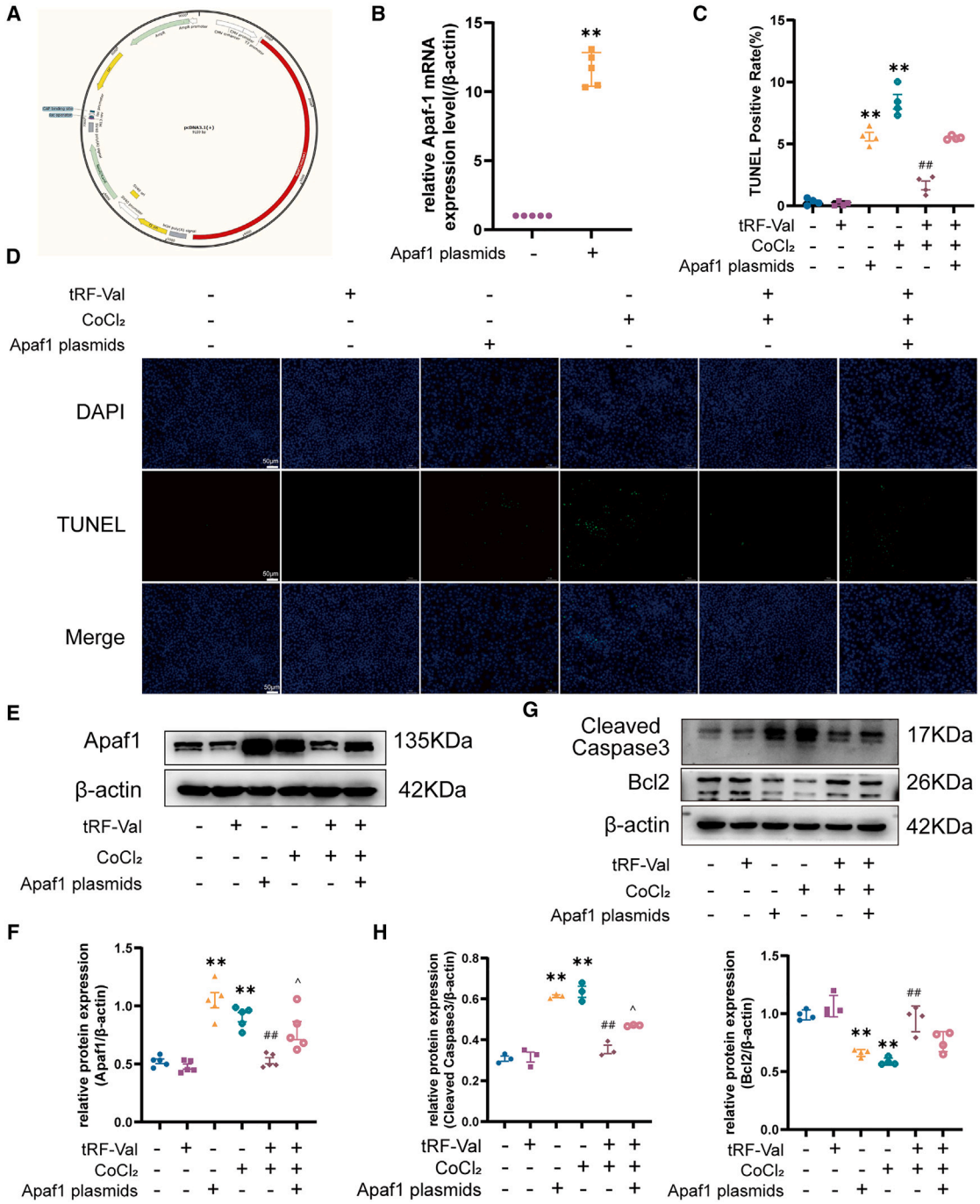

Figure 10. Apaf1 overexpression partly weakens the effect of the tRF-Val on apoptosis in cultured BUMPT cells

(A) Design of the Apaf1 overexpression plasmids, containing 9150 bp.

(B) RT-qPCR result of Apaf1 in group of NC and *Apaf1* plasmids.

(C) Quantitative analysis of TUNEL-positive cells.

(D) Representative images of TUNEL assay of BUMPT cells. Scale Bar, 50 μm.

(E) Western blot analysis of Apaf1 with β-actin as a loading control in BUMPT cells.

(F) Quantitative analysis of Apaf1 in BUMPT cells.

(G) Western blot analysis of Bcl2 and cleaved caspase-3 with β-actin as a loading control in BUMPT cells.

(H) Quantitative analysis of Bcl2 and cleaved caspase-3 in BUMPT cells. Data are represented as mean ± SEM. **, $p < 0.01$ versus respective vehicle; ##, $p < 0.01$ versus NC + $CoCl_2$ group; ^, $p < 0.05$ versus tRF-Val + $CoCl_2$ group. $n \geq 3$.

DECLARATION OF INTERESTS

The authors declare no competing interests.

STAR★METHODS

Detailed methods are provided in the online version of this paper and include the following:

- KEY RESOURCES TABLE
- EXPERIMENTAL MODEL AND STUDY PARTICIPANT DETAILS
  - Animal experiment
  - Cell culture
- METHOD DETAILS
  - Bioinformatic analysis
  - Cell transfection and treatment
  - Detection of tRFs
  - Measurement of blood urea nitrogen (BUN) and serum creatinine (sCr)
  - Histology, TUNEL assay, IHC staining
  - Mitochondria morphology observation by electron microscope
  - Flow cytometry assay
  - mRNA-sequencing
  - Quantitative RT-PCR (RT-qPCR)
  - Western Blot
  - Dual luciferase reporter assay
  - AGO-RIP assay
- QUANTIFICATION AND STATISTICAL ANALYSIS

SUPPLEMENTAL INFORMATION

Supplemental information can be found online at https://doi.org/10.1016/j.isci.2025.111954.

Received: August 29, 2024
Revised: October 22, 2024
Accepted: January 31, 2025
Published: February 5, 2025

REFERENCES

1. Ronco, C., Bellomo, R., and Kellum, J.A. (2019). Acute kidney injury. Lancet *394*, 1949–1964. https://doi.org/10.1016/s0140-6736(19)32563-2.
2. Ardura, J.A., Sanz, A.B., Ortiz, A., and Esbrit, P. (2013). Parathyroid hormone-related protein protects renal tubuloepithelial cells from apoptosis by activating transcription factor Runx2. Kidney Int. *83*, 825–834. https://doi.org/10.1038/ki.2012.476.
3. Sanz, A.B., Sanchez-Niño, M.D., Ramos, A.M., and Ortiz, A. (2023). Regulated cell death pathways in kidney disease. Nat. Rev. Nephrol. *19*, 281–299. https://doi.org/10.1038/s41581-023-00694-0.
4. Ma, T., Li, H., Liu, H., Peng, Y., Lin, T., Deng, Z., Jia, N., Chen, Z., and Wang, P. (2022). Neat1 promotes acute kidney injury to chronic kidney disease by facilitating tubular epithelial cells apoptosis via sequestering miR-129-5p. Mol. Ther. *30*, 3313–3332. https://doi.org/10.1016/j.ymthe.2022.05.019.
5. Gortat, A., Sancho, M., Mondragón, L., Messeguer, À., Pérez-Payá, E., and Orzáez, M. (2015). Apaf1 inhibition promotes cell recovery from apoptosis. Protein Cell *6*, 833–843. https://doi.org/10.1007/s13238-015-0200-2.
6. Kumar, P., Kuscu, C., and Dutta, A. (2016). Biogenesis and Function of Transfer RNA-Related Fragments (tRFs). Trends Biochem. Sci. *41*, 679–689. https://doi.org/10.1016/j.tibs.2016.05.004.
7. Yang, W., Gao, K., Qian, Y., Huang, Y., Xiang, Q., Chen, C., Chen, Q., Wang, Y., Fang, F., He, Q., et al. (2022). A novel tRNA-derived fragment AS-tDR-007333 promotes the malignancy of NSCLC via the HSPB1/MED29 and ELK4/MED29 axes. J. Hematol. Oncol. *15*, 53. https://doi.org/10.1186/s13045-022-01270-y.
8. Ivanov, P., Emara, M.M., Villen, J., Gygi, S.P., and Anderson, P. (2011). Angiogenin-induced tRNA fragments inhibit translation initiation. Mol. Cell *43*, 613–623. https://doi.org/10.1016/j.molcel.2011.06.022.
9. Yamasaki, S., Ivanov, P., Hu, G.F., and Anderson, P. (2009). Angiogenin cleaves tRNA and promotes stress-induced translational repression. J. Cell Biol. *185*, 35–42. https://doi.org/10.1083/jcb.200811106.
10. Li, D., Zhang, H., Wu, X., Dai, Q., Tang, S., Liu, Y., Yang, S., and Zhang, W. (2022). Role of tRNA derived fragments in renal ischemia-reperfusion injury. Ren. Fail. *44*, 815–825. https://doi.org/10.1080/0886022x.2022.2072336.
11. Kumar, P., Mudunuri, S.B., Anaya, J., and Dutta, A. (2015). tRFdb: a database for transfer RNA fragments. Nucleic Acids Res. *43*, D141–D145. https://doi.org/10.1093/nar/gku1138.
12. Mishima, E., Inoue, C., Saigusa, D., Inoue, R., Ito, K., Suzuki, Y., Jinno, D., Tsukui, Y., Akamatsu, Y., Araki, M., et al. (2014). Conformational change in transfer RNA is an early indicator of acute cellular damage. J. Am. Soc. Nephrol. *25*, 2316–2326. https://doi.org/10.1681/asn.2013091001.
13. Khurana, R., Ranches, G., Schafferer, S., Lukasser, M., Rudnicki, M., Mayer, G., and Hüttenhofer, A. (2017). Identification of urinary exosomal noncoding RNAs as novel biomarkers in chronic kidney disease. RNA *23*, 142–152. https://doi.org/10.1261/rna.058834.116.
14. Holderied, A., and Anders, H.J. (2014). t-RNA fragmentation as an early biomarker of (kidney) injury. J. Am. Soc. Nephrol. *25*, 2145–2147. https://doi.org/10.1681/asn.2014040338.
15. Zhang, Z., Qiao, Y., Ji, J., Huang, C., Shi, H., Gan, W., and Zhang, A. (2024). The potential role of differentially expressed tRNA-derived fragments in high glucose-induced podocytes. Ren. Fail. *46*, 2318413. https://doi.org/10.1080/0886022x.2024.2318413.
16. Li, D., Xie, X., Zhan, Z., Li, N., Yin, N., Yang, S., Liu, J., Wang, J., Li, Z., Yi, B., et al. (2024). HIF-1 induced tiRNA-Lys-CTT-003 is protective against cisplatin induced ferroptosis of renal tubular cells in mouse AKI model. Biochim. Biophys. Acta, Mol. Basis Dis. *1870*, 167277. https://doi.org/10.1016/j.bbadis.2024.167277.
17. Cui, H., Li, H., Wu, H., Du, F., Xie, X., Zeng, S., Zhang, Z., Dong, K., Shang, L., Jing, C., and Li, L. (2022). A novel 3'tRNA-derived fragment tRF-Val promotes proliferation and inhibits apoptosis by targeting EEF1A1 in gastric cancer. Cell Death Dis. *13*, 471. https://doi.org/10.1038/s41419-022-04930-6.
18. Wolfs, T.G.A.M., de Vries, B., Walter, S.J., Peutz-Kootstra, C.J., van Heurn, L.W.E., Oosterhof, G.O.N., and Buurman, W.A. (2005). Apoptotic cell death is initiated during normothermic ischemia in human kidneys. Am. J. Transplant. *5*, 68–75. https://doi.org/10.1111/j.1600-6143.2004.00657.x.
19. Yang, H., Zhang, W., Xie, T., Wang, X., and Ning, W. (2019). Fluorofenidone inhibits apoptosis of renal tubular epithelial cells in rats with renal interstitial fibrosis. Braz. J. Med. Biol. Res. *52*, e8772. https://doi.org/10.1590/1414-431x20198772.
20. Orzáez, M., Sancho, M., Marchán, S., Mondragón, L., Montava, R., Valero, J.G., Landeta, O., Basañez, G., Carbajo, R.J., Pineda-Lucena, A., et al. (2014). Apaf-1 inhibitors protect from unwanted cell death in *in vivo* models of kidney ischemia and chemotherapy induced ototoxicity. PLoS One *9*, e110979. https://doi.org/10.1371/journal.pone.0110979.
21. Kuscu, C., Kumar, P., Kiran, M., Su, Z., Malik, A., and Dutta, A. (2018). tRNA fragments (tRFs) guide Ago to regulate gene expression post-transcriptionally in a Dicer-independent manner. RNA *24*, 1093–1105. https://doi.org/10.1261/rna.066126.118.
22. Kumar, P., Anaya, J., Mudunuri, S.B., and Dutta, A. (2014). Meta-analysis of tRNA derived RNA fragments reveals that they are evolutionarily conserved and associate with AGO proteins to recognize specific RNA targets. BMC Biol. *12*, 78. https://doi.org/10.1186/s12915-014-0078-0.
23. Han, Y., Peng, Y., Liu, S., Wang, X., Cai, C., Guo, C., Chen, Y., Gao, L., Huang, Q., He, M., et al. (2022). tRF3008A suppresses the progression

and metastasis of colorectal cancer by destabilizing FOXK1 in an AGO-dependent manner. J. Exp. Clin. Cancer Res. *41*, 32. https://doi.org/10.1186/s13046-021-02190-4.

24. Zhang, M., Li, F., Wang, J., He, W., Li, Y., Li, H., Wei, Z., and Cao, Y. (2019). tRNA-derived fragment tRF-03357 promotes cell proliferation, migration and invasion in high-grade serous ovarian cancer. OncoTargets Ther. *12*, 6371–6383. https://doi.org/10.2147/ott.S206861.
25. Wei, Q., Sun, H., Song, S., Liu, Y., Liu, P., Livingston, M.J., Wang, J., Liang, M., Mi, Q.S., Huo, Y., et al. (2018). MicroRNA-668 represses MTP18 to preserve mitochondrial dynamics in ischemic acute kidney injury. J. Clin. Investig. *128*, 5448–5464. https://doi.org/10.1172/jci121859.
26. Paller, M.S., Hoidal, J.R., and Ferris, T.F. (1984). Oxygen free radicals in ischemic acute renal failure in the rat. J. Clin. Investig. *74*, 1156–1164. https://doi.org/10.1172/jci111524.

STAR★METHODS

KEY RESOURCES TABLE

REAGENT or RESOURCE	SOURCE	IDENTIFIER
Antibodies		
Rabbit monoclonal anti-Apaf1	Cell Signaling Technology	Cat#8723; RRID: AB_3676010
Rabbit monoclonal anti-Apaf1	Beyotime	Cat#AF1462; RRID: AB_3676027
Rabbit polyclonal anti-Apaf1	Affinity	Cat#AF0117; RRID: AB_2833267
Rabbit monoclonal anti-Bcl2	Abcam	Cat#ab182858; RRID: AB_2715467
Rabbit monoclonal anti-Cleaved-Caspase3	Abcam	Cat#ab214430; RRID: AB_2938798
Mouse monoclonal anti-β-actin	Proteintech	Cat#66009-1-Ig; RRID: AB_2687938
goat anti-rabbit IgG-HRP secondary antibody	Abiowell	Cat#AWS0002; RRID: AB_3676031
goat anti-mouse IgG-HRP secondary antibody	Abiowell	Cat#AWS0001; RRID: AB_3676030
Chemicals, peptides, and recombinant proteins		
Dulbecco's Modified Eagle's Medium	Gibco	Cat#C11995500BT
Fetal bovine serum	Procell LifeScience & Technology	Cat#164210-50-1
Streptomycin-penicillin	Wuhanhuiyucheng Biotechnology	Cat#HYG2222
Lipofectamine 3000	ThermoFisher Scientific	Cat#L3000015
Cobalt chloride hexahydrate	Rhawn Reagent	Cat#7791-13-1
Critical commercial assays		
TUNEL cell death detection kit	Beyotime	Cat#C1088
Annexin V-FITC and PI apoptosis assay kit	Beyotime	Cat#C1062
HiScript II qRT SuperMix(+gDNA Wiper)	Vazyme	Cat#R223
ChamQ Universal SYBR qPCR Master Mix Kit	Vazyme	Cat#Q711
miRNA 1st-strand cDNA Synthesis Kit	Vazyme	Cat#MR101
miRNA Universal SYBR qPCR Master Mix	Vazyme	Cat#MQ101
Deposited data		
tsRNAs raw and analyzed data	Li et al.[10]	N/A
mRNA sequencing analyzed data	This study	GSE282997
Experimental models: Cell lines		
BUMPT-306 cells	Department of Nephrology, The Third Xiangya Hospital, Central South University	RRID: CVCL_D3WF
HEK-293T cells	Department of Nephrology, The Third Xiangya Hospital, Central South University	RRID: CVCL_0063
Experimental models: Organisms/strains		
C57BL/6J Mouse	Slyke Jingda Biotechnology Company	RRID: IMSR_JAX:000664
Oligonucleotides		
tRF-Val sequence: 5'- CAAUGAACACUCUGACCA -3'	This paper	N/A
tRF-Val inhibitor sequence: 5'- UGGUCAGAGUGUUCAUUG-3'	This paper	N/A
Primers for tRF-Val, see Table 1	This paper	N/A
Primers for U6, see Table 1	Li et al.[16]	N/A
Primers for Apaf1, see Table 2	This paper	N/A
Primers for β-actin, see Table 2	Li et al.[16]	N/A
Recombinant DNA		
Apaf1 pcDNA3.1 plasmid	This paper	N/A
Apaf1 3'-UTR psiCHECKTM-2 plasmid (wild type)	This paper	N/A
Apaf1 3'-UTR psiCHECKTM-2 plasmid (mutant type)	This paper	N/A

(*Continued on next page*)

Continued

REAGENT or RESOURCE	SOURCE	IDENTIFIER
Software and algorithms		
ImageJ	This paper	RRID:SCR_003070
GraphPad Prism	This paper	RRID:SCR_002798
Flowjo	This paper	RRID:SCR_008520
ZEISS ZEN Microscopy Software	This paper	RRID:SCR_013672

EXPERIMENTAL MODEL AND STUDY PARTICIPANT DETAILS

Animal experiment

C57BL/6J male mice (20-25 g, 8 weeks old) were purchased from Slyke Jingda Biotechnology Company (Certificate SYXK2019-0004; Hunan, China). The mice were randomly allocated into the Sham group and bilateral IRI model group (n = 5 per group). A bilateral IRI model was established according to a previous study.[25] The mice model of renal bilateral IRI was established using two microvascular clamps for 30 min followed by reperfusion without contralateral nephrectomy. Sham mice underwent the same surgical procedure without clamping. 24 hours prior to surgery, caudal vein injections of either scrambled or *in vivo*-optimized tRF-Val or tRF-Val inhibitor (10 mg/kg) were administered. Mice were sacrificed 24 or 48 hours post-bilateral IRI, and both kidney tissues and serum were collected for various analysis. This study was reviewed and carried out in Department of Laboratory Animals of Central South University. All experiments using animals were conducted in strict accordance with the approved guidelines by the Laboratory Animal Ethics Committee of Central South University (CSU-2023-0259).

Cell culture

BUMPT cells line was provided by the Institute of Nephrology, Central South University. BUMPT cells were cultured in DMEM supplemented with 10% FBS, 1% streptomycin-penicillin at 37°C with 5% CO_2. And there was no mycoplasma contamination under microscopic observation.

METHOD DETAILS

Bioinformatic analysis

Heatmap and volcano plot analyses were conducted utilizing R language and bioinformatics.com.cn to identify differentially expressed tsRNAs between IRI and Sham samples. Building upon preliminary work by our research team, this study utilized previously published tRFs & tiRNAs sequencing data for bioinformatic analysis.[10]

Cell transfection and treatment

BUMPT cells with 50% confluence was transfected using Lipofectamine 3000 according to the manufacturer's protocol. Briefly, cells (4×10^5 cells) were seeded onto 6-well plates. Then, the cells were cultured in Opti-Minimum Essential Media (OPTI-MEM) reduced serum medium containing tRF-Val mimic or inhibitor. After incubation for 24 h, BUMPT cells were treated with 400 μM $CoCl_2$ for 48 h to induce hypoxia and incubated in fresh complete medium.

tRF-Val, 5'- CAAUGAACACUCUGACCA -3', tRF-Val inhibitor, 5'- UGGUCAGAGUGUUCAUUG-3'.

Detection of tRFs

Total RNA was extracted from mouse kidney tissues and BUMPT cells using the TransZol UP RNA Extraction Kit. tRFs were pretreated by rtStar™ tRF & tiRNA Pretreatment Kit (Arraystar, AS-FS-005, USA) according to the manufacturer's instruction. The miRNA 1st-strand cDNA Synthesis Kit (Vazyme, MR101, Nanjing, China) was used to perform polyadenylation reactions and cDNA synthesis. Later, miRNA Universal SYBR qPCR Master Mix (Vazyme, MQ101, Nanjing, China) was used to measure the expression of tRFs. We determined the level of expression of tRF-Val using standard curve method and cycle threshold (CT) values, and U6 sncRNA expression was used to normalize the expression of tRF-Val. Relative quantification of tRF-Val was analyzed using the $2^{-\Delta\Delta CT}$ method. The sequence of the primer used for PCR was listed as follows in Table 1.

Measurement of blood urea nitrogen (BUN) and serum creatinine (sCr)

Collected mouse blood samples were centrifuged, and the serum was obtained for biochemical assays. The urea nitrogen test kit and creatinine test kit were purchased from Hunan Haiyuan Medical. The concentrations of blood urea nitrogen and serum creatinine were measured following the manufacturer's instructions and using autoanalyzer of the Third Xiangya Hospital.

Histology, TUNEL assay, IHC staining

According to routine protocols, the histological sections of the kidney (4μm) were dyed with HE and PAS staining to observe morphological changes. The degree of renal interstitial injury in mice was assessed as previously reported including TECs morphology, brush border integrity, the number of renal epithelial casts, and lumen necrotic cells.[26] Apoptosis of renal TECs was examined by TUNEL assay kit according to the manufacturer's instructions and DAPI was used to stain the nuclei. IHC staining was used to detect the expression of Apaf1 in renal tissue. After blocking with 5% bovine serum albumin (BSA), the renal tissue sections were incubated overnight at 4°C with Anti-Apaf1 rabbit polyclonal antibody (1:100 dilution). Semiquantitative analysis was performed independently by two blinded pathologists.

Mitochondria morphology observation by electron microscope

$1mm^3$ of fresh kidney cortex was quickly placed in electron microscope fixative (Glutaraldehyde, 4%) at 4°C. Then the tissue was embedded and cut into ultrathin sections of 60-80 nm, followed by uranium-lead double staining. The morphology of mitochondria in proximal renal TECs was observed by TEM and images of different multiples were collected.

Flow cytometry assay

Annexin V-FITC and PI staining was conducted to assess apoptosis according to the manufacturers' instruction (Beyotime, C1062, China) then immediately detected by flow cytometer. And the results were analyzed by Flowjo v10.8.6 software.

mRNA-sequencing

mRNA-sequencing was carried out to identify the downstream target genes regulated by tRF-Val. BUMPT cells were transfected with tRF-Val or NC for 48 hours. Thereafter, RNA was isolated from the treated BUMPT cells using the TRIzol reagents (Invitrogen, Shanghai, China). RNA-seq libraries and sequencing were performed on an Illumina HiSeq 4000 by Aksomics (Shanghai, China) and sequencing reads were trimmed using StringTie and mapped to mouse genome database (GRCh37) by the Hisat2 software. Differential expression and normalized read counts (FPKM, Fragments per kilobase of gene/transcript model per million mapped fragments) were calculated using the Ballgown software. The mRNA sequencing data have been deposited to GEO dataset (GSE282997).

Quantitative RT-PCR (RT-qPCR)

First cDNA was synthesized by HiScript II qRT SuperMix(+gDNA Wiper) (Vazyme, R223, Nanjing, China) for qPCR. Real-time fluorescent quantitative PCR was performed based on instructions of the ChamQ Universal SYBR qPCR Master Mix Kit (Vazyme, Q711, Nanjing, China) The preparation of the reaction system and procedure were conducted according to the instructions. Gene expression relative to internal controls was quantified using the $2^{-\Delta\Delta CT}$ method. The PCR primers are shown in Table 2.

Western Blot

The extracted proteins were separated from total proteins by SDS/ PAGE and electro-transferred to PVDF membranes (Millipore, IPVH00010, USA). Membranes were blocked with 0.1% BSA solution on shaker for 1h, then incubated with corresponding primary antibody overnight at 4°C, finally incubated with chemical secondary antibodies for 1h at room temperature the next day. Membranes were visualized by Image Studio software and band intensities were quantitatively analyzed by Image J analysis software. All data represent at least three independent experiments.

Dual luciferase reporter assay

The full-length 3'-UTR of Apaf1 carrying mutant or wild-type sequences was cloned into psiCHECKTM-2 vectors (Promega, MWI, USA), respectively, and co-transfected with tRF-Val overexpression vector or mock vector into HEK-293T cells, using Lipofectamine 3000. After 48h of transfection, the activities of firefly and Renilla luciferase were measured using the dual-luciferase reporter gene assay system (Promega, MWI, USA) in accordance with the manufacturer's protocols.

AGO-RIP assay

The RIP experiment was conducted by Aksomics (Shanghai, China) using the EZ-Magnetic RIP kit (Millipore, MA, USA) according to the manufacturer's instructions. Briefly, cells at 80% confluency were lysed in complete RIP lysis buffer, following by immunoprecipitation with RIP buffer including magnetic beads coupled with anti-AGO antibody (Abcam) at 4°C for 3 h with rotation. Anti-IgG was used as a negative control. Those unbound substances were washed off after the fixed magnetic beads combined complexes with magnet. The samples were co-incubated with proteinase K to purify RNA then the immunoprecipitated RNA was isolated, and the precipitate was analyzed for tRF-Val level by RT-qPCR.

QUANTIFICATION AND STATISTICAL ANALYSIS

Continuity variables were presented as mean ± Standard Error of the Mean (SEM) and analyzed by GraphPad Prism 9 software (San Diego, CA, USA). Student t-test was used to establish statistical significance between two groups (in Figures 1, 6, and 9), and one-way ANOVA followed by Dunnett's post-hoc test was applied among groups of more than two (in Figures 2, 3, 4, 5, 7, 8, 10, and S1). $n \geq 3$ indicates number of animals (Figures 2B, 2F, 2H, 2J, 3B, 3F, 3H, 3J, 7B, and 8B) or biological replicates (except above mentioned). Error bars on all graphs indicate SEM. $P < 0.05$ was considered statistically significant.